Influence of the Sodium Impregnation Solvent on the Deactivation of Cu/FER-Exchanged Zeolites Dedicated to the SCR of NOx with NH3

Marie-Laure Tarot, Mathias Barreau, Daniel Duprez, Vincent Lauga, Eduard Iojoiu, Xavier Courtois, Fabien Can

catalysts

MDPI

Article

Influence of the Sodium Impregnation Solvent on the Deactivation of Cu/FER-Exchanged Zeolites Dedicated to the SCR of NO_x with NH_3

Marie-Laure Tarot [1], Mathias Barreau [1], Daniel Duprez [1], Vincent Lauga [2], Eduard Emil Iojoiu [2], Xavier Courtois [1,*] and Fabien Can [1,*]

1 CNRS, UMR 7285 Institut de Chimie des Milieux et Matériaux de Poitiers (IC2MP), Université de Poitiers, 4 rue Michel Brunet—TSA 51106—86073 Poitiers CEDEX 9, France; marie.laure.tarot@univ-poitiers.fr (M.-L.T.); mathias.barreau@univ-poitiers.fr (M.B.); daniel.duprez@univ-poitiers.fr (D.D.)

2 Renault Trucks—Volvo Group Trucks Technology—Powertrain Engineering Lyon, 99 route de Lyon—69806 Saint-Priest CEDEX, France; vincent.lauga@volvo.com (V.L.); eduard.emil.iojoiu@volvo.com (E.E.I.)

* Correspondence: xavier.courtois@univ-poitiers.fr (X.C.); fabien.can@univ-poitiers.fr (F.C.); Tel.: +33-519453994 (X.C.); +33-549453997 (F.C.)

Received: 24 November 2017; Accepted: 19 December 2017; Published: 23 December 2017

Abstract: The effect of the sodium addition mode was investigated on model Cu/FER selective catalytic reduction (SCR) catalysts with two copper loadings (2.8 wt. % and 6.1 wt. %) in order to compare samples with or without over-exchanged copper. Na was added by wet-impregnation using two solvents: water or ethanol. Catalysts were evaluated in Standard and Fast-SCR conditions, as well as in NO and NH_3 oxidation. They were characterized by H_2-TPR, NO and NH_3 adsorption monitored by FT-IR. As expected, whatever the copper loading, ammonia adsorption capacity was decreased by Na additions. Interestingly, characterizations also showed that Na impregnation in water favors the migration of the Cu-exchanged species, leading to the formation of CuO extra-framework compounds. Consequently, for both copper loadings, Na impregnation in water led to a stronger catalyst deactivation than impregnation in ethanol. Finally, the NO_x conversion at low temperature (250 °C) appeared mainly affected by the loss in NH_3 adsorption capacity whereas the deNO_x deactivation at high temperature (500 °C) was rather governed by the decrease in the exchanged copper ratio, which also induced a partial inhibition of NO and NH_3 oxidation behaviors.

Keywords: NH_3-SCR; sodium poisoning; copper exchanged zeolite; acidity

1. Introduction

Selective catalytic reduction of NO_x by ammonia (NH_3-SCR) is an effective method to control nitrogen oxides emissions from fixed-source exhaust gases. The main involved reactions are the "Standard-SCR" reaction (Equation (1)) and the "Fast-SCR" reaction (Equation (2)).

$$2NH_3 + 2NO + ½O_2 \rightarrow 2N_2 + 3H_2O \quad (1)$$

$$2NH_3 + NO + NO_2 \rightarrow 2N_2 + 3H_2O \quad (2)$$

In fact, the activity obtained in Standard-SCR condition is largely improved by favoring the oxidation of NO to NO_2 to provide the most favorable NO_2/NO_x ratio of 0.5, leading to the "Fast-SCR" stoichiometry.

More recently, this NH_3-SCR technology was adapted to mobile sources to reach the environmental standards dedicated to passenger cars and heavy duty vehicles. Ammonia is then

usually obtained by the decomposition of an aqueous solution of urea, which is injected in the exhaust pipe. The first generations of NH_3-SCR catalysts were based on V_2O_5-WO_3-TiO_2 materials, as usually implemented for NO_x treatment from power plants and stationary sources. Subsequently, new systems have emerged to expand the operating temperature window and to solve the high temperature deactivation drawback due to the anatase-rutile transition of TiO_2 and the possible V_2O_5 sublimation. Metal-exchanged zeolite-based catalysts were reported to be relevant materials for this purpose. A variety of zeolites have been proposed (ZSM-5, mordenite, beta, ferrierite, Y-zeolite, chabazite, ...) and in the last few years, new generations of exchanged catalysts based on small pore zeolites have emerged. For instance, SAPO-34 or SZZ-13-based zeolites showed very good hydrothermal stabilities and also a resistance to hydrocarbon (HC) poisoning [1–4]. Zeolites are usually promoted by transition metals such as iron or copper [5]. Compared with iron-exchanged zeolites, copper-zeolite catalysts were reported to be more active at low temperature (<300 °C), less sensitive to the inlet NO_2/NO_x ratio, but produced more N_2O [6].

Besides, CO_2 emissions from common fossil sources induce a worrying situation that requires to increase the role of renewable resources for energy production. Biomass can be used as feedstock for the production of biodiesel which can be then utilized in the transport sector to replace fossil fuels. According to the recent European legislation (Directive 2003/30/EC), 10% share of biofuels in the transport sector must be achieved by 2020. However, biodiesel contains minerals traces such as sodium, potassium or phosphorus, which are authorized in limited amounts (maximum of 5 and 4 ppm for Na + K and P, respectively in European Union; EN 14214). Considering that (i) the Euro VI standard for heavy duty vehicles requires a durability of 700,000 km and (ii) some truck fleets use biodiesel exclusively, catalysts in the exhaust pipe may be subjected to kilograms of these poisons. Consequently, this study is focused on the influence of Na deposit on the NH_3-SCR process over copper-exchanged zeolite.

The effects of alkali on vanadia-based SCR catalysts are well described in the literature. For instance, exchange of alkali metal cation from the acids groups of V-OH species decreases the acidity, leading to a loss of ammonia-sorption properties [7]. The deactivation of the V^{5+} = O redox sites was also highlighted [8]. In addition, potassium was reported to induce a stronger deactivation than sodium, for four similar weight contents of sodium and potassium (0.1, 0.5, 1, 2 wt. %) in the same catalyst [9]. Similar conclusion was reported by Kern et al. [10] for iron-exchanged catalysts with K and Na contents from 0 to 0.5 $mmol/g_{cata}$. However, only few studies concerning the poisoning of zeolites by alkali are available. Sodium and potassium are supposed to lead to the same type of deactivation. Shwan et al. studied the poisoning of a Fe-BEA zeolite by exposition to vapors from an aqueous solution of KNO_3 [11]. This poisoning led to a decrease in the Brønsted acidity and to a loss of active isolated iron species, but also increased both the NO_x storage behavior and the NO oxidation activity. Ma et al. [12] observed the same tendencies on the Cu/SAPO-34 poisoned by incipient wetness impregnation. They also noticed that the Standard-SCR activity is not impacted with 0.5 wt. % of potassium. Adding potassium firstly affected the low temperature activity (<300 °C) together with an increase in the N_2O formation. In addition, Brookshear et al. [13,14] showed the importance of the diesel exhaust pipe design toward the sodium impact on the SCR catalyst. The heavy duty configuration (Diesel Oxidation Catalyst (DOC)—Diesel Particulate Filter (DPF)—SCR) was less impacted by sodium than in the light-duty configuration (DOC-SCR-DPF), because sodium was preferentially trapped by the DPF.

The aim of this study was to investigate the deactivation of Cu-FER catalysts by sodium, with a special focus on the influence of the sodium impregnation solvent. The ferrierite (FER) structure was selected as host support because of its medium pore size allowing a high thermal stability [15]. FER structure was also claimed as appropriate structure for iron or copper-exchanged SCR catalysts [16]. Impregnation of sodium in water was used especially to simulate cold start/engine switch off periods, for which water condensation occurs in the exhaust pipe [11,12,17]. However, the use of such polar solvent should not be representative of Na-catalyst interactions in the exhaust pipe at usual operating

temperature. Then, sodium impregnations were also performed in ethanol, which is less polar than water, to avoid interactions between water and the exchanged zeolite. This is assumed to be more representative of a gas phase poisoning. In order to compare the different mechanisms of deactivation depending on the Na impregnation solvent, two catalysts with or without extra-framework copper were used, containing 6.1 wt. % and 2.8 wt. % of copper, respectively.

2. Results

2.1. Structural/Textural Characterisation of the Catalysts, Elemental Analysis

2.1.1. Sodium Free Catalysts

XRD patterns of the zeolite as received and after the hydrothermal treatment at 600 °C are reported in Supplementary Materials (Figure S1). No evolution of the diffraction peaks were evidenced, which is also consistent with the stability of the specific surface area at 395–405 $m^2 \cdot g^{-1}$. However, the infrared structural band (T–O–T vibrations) were shifted from 1096 to 1103 cm^{-1} after aging, indicating a small dealumination of the zeolite (Supplementary Materials, Figure S2).

After copper exchange, no evolution of the zeolite structure was observed by XRD analysis. No new diffraction peak appeared over $Cu_{2.8}$/FER, whereas broad diffraction peaks appeared on the diffractogram of $Cu_{6.1}$/FER near 2θ = 35.5° and 38.7°, which are attributed to CuO (Supplementary Materials, Figures S3 and S4). For both copper loadings, metal exchange and subsequent hydrothermal treatment induced a decrease of about 10% of the specific surface area, at around 352 m^2 g^{-1} for $Cu_{2.8}$/FER and $Cu_{6.1}$/FER (Table 1).

Table 1. Catalysts characterizations.

[Cu] (wt. %)	n_{Cu}/n_{Al}	Na Impregn Solvent	[Na] (ppm/μmol g^{-1})	n_{Na}/n_{Al}	S_{BET} (m^2 g^{-1})	Vμ [(i)] (cm^3 g^{-1})	Vtotal [(ii)] (cm^3 g^{-1})	H_2-TPR (n_{H2}/n_{Cu})	L:B [(iii)]
2.8 ($Cu_{2.8}$/FER)	0.30	**Na free sample**	**0**	**0**	**352**	**0.12**	**0.22**	**1.02**	**83:17**
		Water (W)	4500/195	0.13				0.98	91:9
			5400/235	0.16				1.00	96:4
			12,800/560	0.37				1.03	100:0
			19,000/830	0.56	270	0.11	0.17	1.04	100:0
		Ethanol (Et)	3900/170	0.11				1.05	91:9
			9600/420	0.28				1.02	89:11
			14,200/620	0.41	238	0.06	0.17	1.10	92:8
6.1 ($Cu_{6.1}$/FER)	0.67	**Na free sample**	**0**	**0**	**352**	**0.12**	**0.23**	**1.03**	**96:4**
		Water (W)	4300/190	0.12				1.03	97:3
			11,800/515	0.34				1.02	100:0
			13,800/600	0.40				1.08	100:0
			20,300/885	0.59	265	0.09	0.16	1.02	100:0
		Ethanol Et)	8700/380	0.25				1.06	98:2
			15,200/665	0.44	251	0.09	0.15	0.96	99:1

[(i)]: microporous volume deduced from N_2 adsorption/desorption at 77 K; [(ii)]: total porous volume deduced from N_2 adsorption/desorption at 77 K; [(iii)]: Lewis acid sites (L); Brønsted acid sites (B) ratio determined by NH_3 adsorption at 50 °C.

2.1.2. Na Impregnated Catalysts

All the sodium loading from Inductively Coupled Plasma (ICP) elemental analysis are reported in Table 1 depending on the copper content and the Na impregnation solvent.

For each $Cu_{2.8}$/FER and $Cu_{6.1}$/FER catalyst, four Na loadings from 4300–4500 ppm to 19,000–20,300 ppm were obtained by sodium impregnation in water. The specific surface areas of the highest loaded samples were decreased to 265–270 m^2 g^{-1}, compared with 352 m^2 g^{-1} for the fresh catalysts (Table 1). In addition, the XRD patterns of the corresponding samples point out the appearance of CuO for $Cu_{2.8}$/FER whereas the intensity of the CuO peaks significantly increased for $Cu_{6.1}$/FER (Supplementary Materials Figures S3 and S4).

Sodium loadings after impregnation in ethanol were ranked between 3900–14,200 ppm and 8700–15,200 ppm for $Cu_{2.8}$/FER and $Cu_{6.1}$/FER, respectively. No evolution of the XRD patterns was observed compared with the sodium free catalyst (patterns not shown), unlike the impregnation of Na in water. This first result already predicts an effect of the sodium solvent toward physico-chemical properties of the materials. The specific surface areas for the higher Na amounts decreased to 240–250 $m^2\ g^{-1}$ (Table 1).

2.2. Catalytic Activity

NO_x conversions obtained over stabilized $Cu_{2.8}$/FER and $Cu_{6.1}$/FER samples (without sodium) are reported in Figure 1 for the Standard-SCR and Fast-SCR conditions. Please remind that the catalytic tests in Fast-SCR condition were performed with lower amount of catalyst (15 mg versus 50 mg for the Standard-SCR condition) to limit the deNO_x efficiency and to possibly distinguish a deactivation by sodium addition.

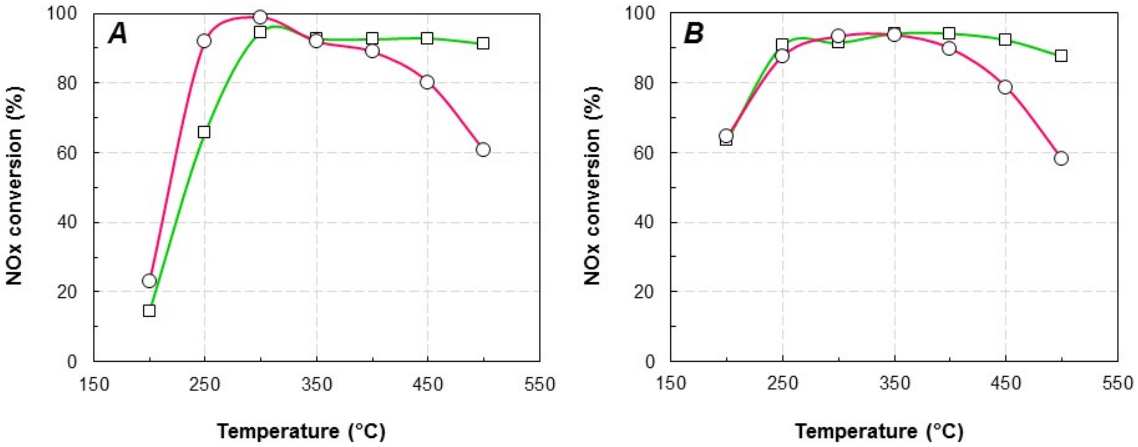

Figure 1. NO_x conversion by NH_3 over Cu/FER-exchanged zeolite. (**A**) standard-SCR; (**B**) Fast-SCR. (—, □): $Cu_{2.8}$/FER; (—, ○): $Cu_{6.1}$/FER.

In Standard-SCR condition (Figure 1A), the best activity at low temperature was achieved by the $Cu_{6.1}$/FER catalyst with a full NO_x conversion at around 300 °C. However, the NO_x conversion showed a net drop in the 350–500 °C temperature range. It is assigned to a competition between the NO_x reduction reaction and the ammonia oxidation reaction, leading to a lack in ammonia to reduce NO_x. To the opposite, $Cu_{2.8}$/FER sample presented an expanded operating temperature window, with around 90–95% of NO_x conversion from 300 to 500 °C. The maximum outlet N_2O concentration was recorded at 500 °C, at 1.5 and 5 ppm for $Cu_{2.8}$/FER and $Cu_{6.1}$/FER, respectively.

Compared with the Standard-SCR condition, higher NO_x conversions were observed at low temperature (200 °C) in Fast-SCR condition (Figure 1B), especially taking into account that the implemented catalyst weight was divided by more than 3. Again, a decrease in NO_x conversion was denoted at temperature higher than 350–400 °C, especially for $Cu_{6.1}$/FER samples, attributed to the ammonia oxidation reaction. The maximum outlet N_2O concentration (500 °C) was then a little increased, at 4 and 7 ppm for $Cu_{2.8}$/FER and $Cu_{6.1}$/FER, respectively.

Standard-SCR and Fast-SCR catalytic tests were also performed on the Cu/FER zeolite containing various sodium loadings. Preliminary tests were performed with catalysts submitted to the impregnation procedures in water or ethanol, but without sodium salt. Results (not shown) indicated no change in the catalytic behavior.

In order to illustrate the influence of both sodium content and sodium impregnation solvent (water or ethanol) on the deNO_x efficiency of both $Cu_{2.8}$/FER and $Cu_{6.1}$/FER catalysts, two representative temperatures were selected: 250 °C was chosen to compare the deNO_x behaviors at “low” temperature,

while 500 °C was selected for the "high" temperature comparisons. Figure 2 compares the loss of the NO_x conversion (expressed as a percentage of loss compared with the Na free samples) at "low" and "high" selected temperatures, depending on the sodium content (water and ethanol solvents are presented in blue and red lines, respectively). Note that the N_2O outlet concentration was not affected by sodium additions.

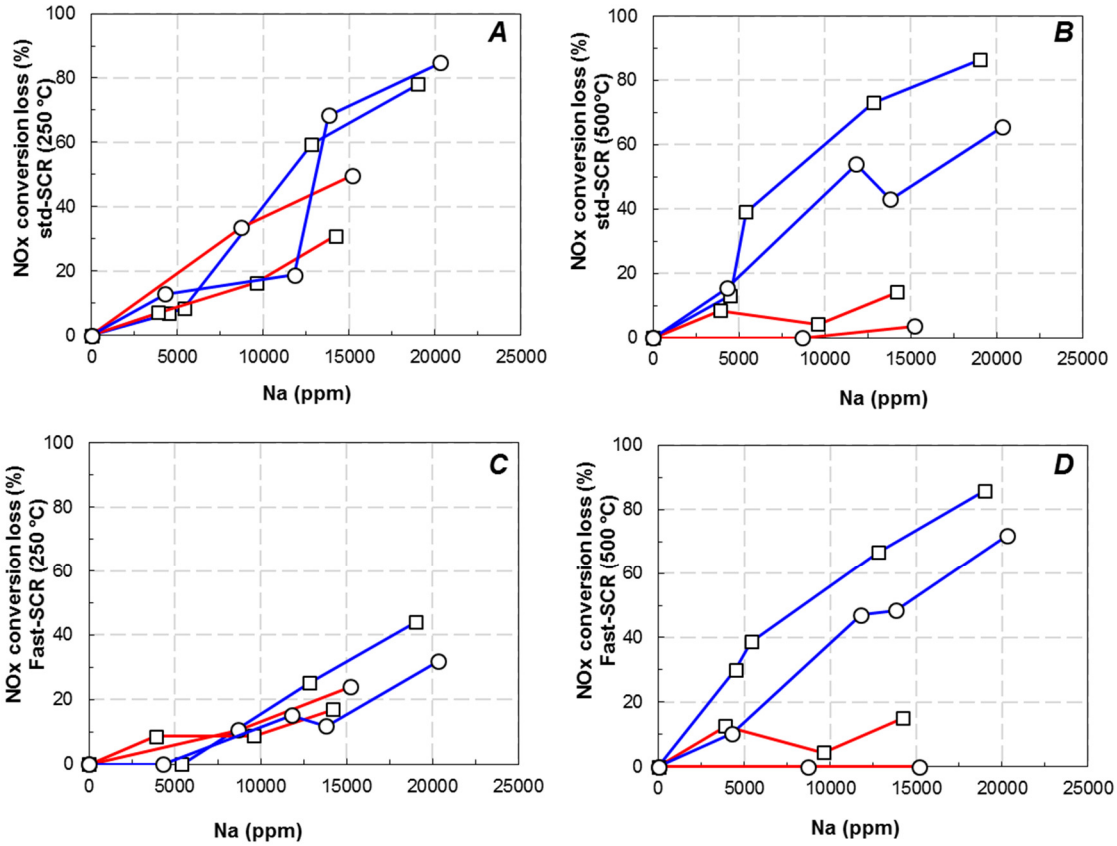

Figure 2. NO_x conversion loss in function of the sodium loading on Cu/FER zeolites in standard (**A**,**B**) and Fast-SCR (**C**,**D**) at 250 °C (**A**,**C**) and 500 °C (**B**,**D**). □: $Cu_{2.8}$/FER; ○: $Cu_{6.1}$/FER. (Na impregnation in water: blue line; sodium impregnation in ethanol: red line).

It appears that the NO_x conversion was strongly affected by the sodium loading. However, the deactivation acted differently depending on both the Na solvent (i.e., water or ethanol) and the SCR inlet condition (Standard or Fast-SCR experiments).

In Standard-SCR condition, when sodium was impregnated on $Cu_{6.1}$/FER via the water pathway (blue line), the deactivation at 250 °C (Figure 2A) appeared rather limited until 12,500 ppm of Na content, with a loss of NO_x conversion of 20%. Beyond, the deNO_x efficiency rapidly dropped to achieve deactivation over 80% for the higher Na content (around 2% of Na deposit). Interestingly, Na deposition using ethanol as solvent (red line) led to different observations. For approximately the same Na content (15,000 ppm), the loss in NO_x conversion was around 50% when sodium was impregnated in ethanol versus 70% when sodium was impregnated in water.

Over $Cu_{2.8}$/FER, same trends were obtained: the most pronounced decrease was observed for sodium impregnation in water (blue line). However, for this catalyst with the low copper loading, the influence of the sodium solvent appeared a little less marked than for $Cu_{6.1}$/FER.

Finally, for Na contents higher than 14,200 ppm impregnated in water, similar NO_x conversions were observed in Standard-SCR condition whatever the catalyst (i.e., $Cu_{6.1}$/FER or $Cu_{2.8}$/FER).

This suggests that beyond a threshold value of Na deposit, both catalysts tend to exhibit similar remaining active sites.

At high temperature, it was previously described that the competitive reaction between ammonia oxidation and NO_x reduction was enhanced over the most loaded copper catalyst ($Cu_{6.1}$/FER). Nevertheless, Figure 2B clearly shows that at 500 °C, for both studied copper loading, sodium impregnation in ethanol (red lines) had few impact on the NO_x conversion up to 14,200 ppm Na content. On the opposite, strong deactivations were denoted when Na was impregnated in water (blue line). The NO_x conversion loss for approximately 2% Na then reached 65% and 86% for $Cu_{6.1}$/FER and $Cu_{2.8}$/FER, respectively.

In Fast-SCR condition, no influence of Na deposits on the NO_2 availability (from NO oxidation into NO_2) is expected since the optimal inlet NO_2/NO_x ratio is already fixed to 0.5. Only other parameters should be involved in the deactivation mechanism. In fact, Figure 2C reports that the NO_x conversion at 250 °C was decreased with similar tendencies with sodium contents, whatever the Na impregnation route (water or ethanol) and regardless the copper loading ($Cu_{2.8}$/FER or $Cu_{6.1}$/FER). The decrease rate appeared less marked than in Standard-SCR condition.

At 500 °C (Figure 2D), similar behaviors to those denoted in Figure 2B (Standard-SCR) are observed: the ethanol impregnation solvent did not induce a strong deactivation of the catalysts whereas impregnation with water induced the same NO_x conversion loss than in Standard-SCR condition.

Finally, for the two studied catalysts with different copper loadings, the sodium impregnation in water strongly impacted the catalytic activity compare with the impregnation in ethanol. Moreover, when Na was added in water, almost the same catalytic activities were reached for the highest sodium loadings for both catalysts with different copper contents, whereas the initial catalytic activities were different. Considering the needed functions for the NH_3-SCR activity, the decrease in activity of the catalysts could be attributed to alteration of the redox properties and/or to a poisoning of the acidic sites. Results described in this section, indicate that sodium addition in water or ethanol did not led to the same effects on the catalysts behaviors. Consequently, dedicated characterizations were performed to gain information about the Na poisoning and the influence of the Na impregnation solvent.

2.3. Redox Properties and Copper Characterization

In this section, the influence of the sodium impregnation solvent was examined through redox properties of $Cu_{2.8}$/FER and $Cu_{6.1}$/FER catalysts. Both NH_3 and NO oxidation catalytic tests and H_2-TPR experiments were carried out. Additionally, NO adsorption monitored by infrared spectroscopy was also performed to assess to the copper state.

2.3.1. NH_3 and NO Oxidation

As described in the previous section, the oxidation performances of $Cu_{2.8}$/FER and $Cu_{6.1}$/FER are suspected to be differently affected by the sodium loading and impregnation solvent. Catalytic oxidation of NH_3 and NO experiments were then performed over all the studied samples. The ammonia oxidation by oxygen is not expected since it induces an undesired reductant consumption, but it also accounts for ammonia activation. NO oxidation is mainly involved in Standard-SCR condition to promote the Fast-SCR stoichiometry. Experiments were performed from 300 °C up to 500 °C for ammonia oxidation and from 350 °C up to 500 °C for NO oxidation, but only data recorded at 450 °C are reported in Figure 3 as representative results.

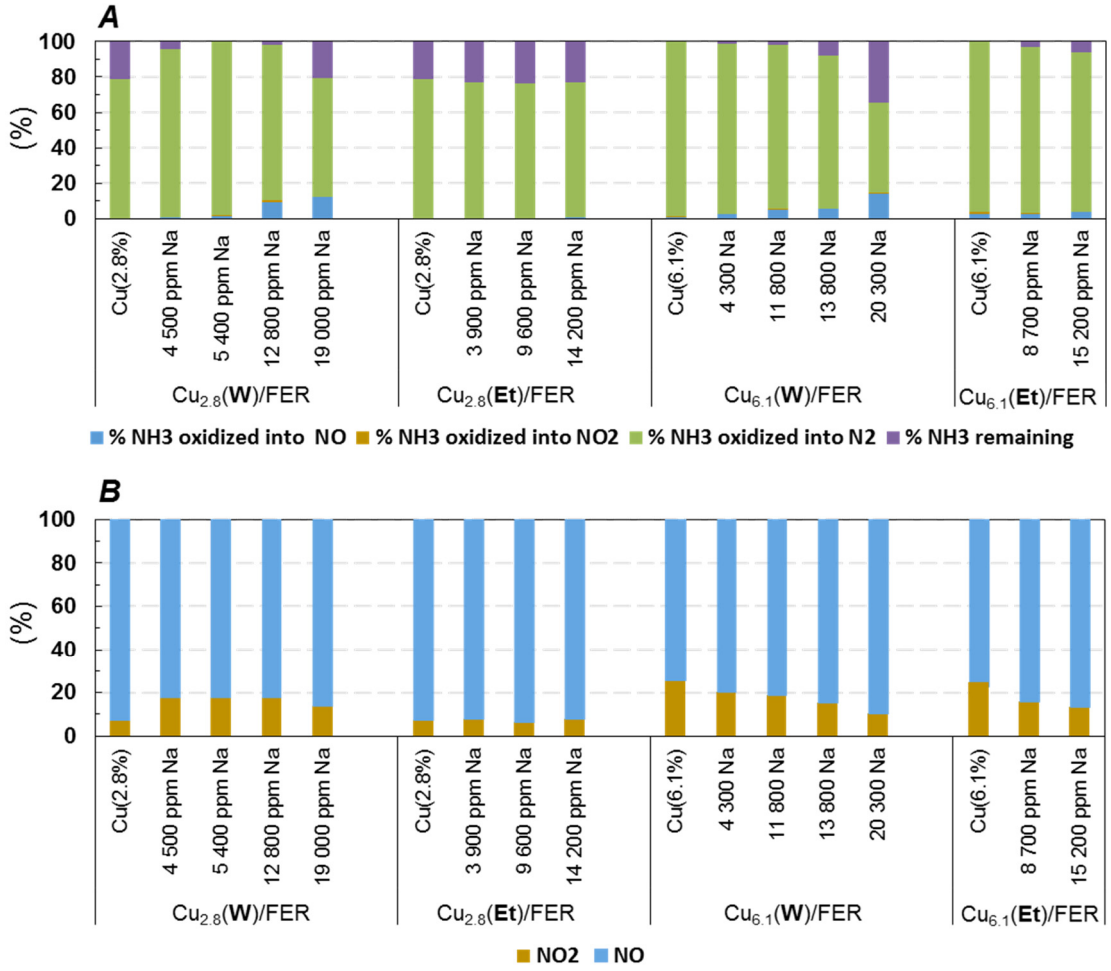

Figure 3. Effect of Na loading on NH_3 (**A**) and NO (**B**) oxidation activities at 450 °C over $Cu_{2.8}$/FER and $Cu_{6.1}$/FER, depending on the Na loading impregnated in water (W) or ethanol (Et).

With sodium free samples, full ammonia oxidation was observed with the highest loaded copper catalyst ($Cu_{6.1}$/FER, Figure 3A). The ammonia oxidation then appeared fully selective in N_2 since neither NO_x nor N_2O were recorded (detection limits close to 1 ppm for these N-products). To the opposite, 78% of NH_3 was converted over $Cu_{2.8}$/FER sample. These results are in accordance with SCR tests presented Figure 1 which illustrate that the competitive reactivity between NH_3 oxidation by O_2 and NO_x reduction by NH_3 at high temperature is more significant over the $Cu_{6.1}$/FER catalyst. Both NH_3 oxidation activity and selectivity were impacted by Na poisoning. Concerning the $Cu_{2.8}$/FER catalyst, Na deposits in water ($Cu_{2.8}$(W)/FER) firstly enhanced the NH_3 conversion into N_2. Increasing the sodium content at 12,800 ppm led to NO formation which was also associated with a decrease in the NH_3 conversion, especially for 19,000 ppm Na. To the opposite, sodium impregnation in ethanol ($Cu_{2.8}$(Et)/FER) did not alter the oxidation of NH_3 by O_2. For $Cu_{6.1}$/FER sample, both Na impregnations in water or ethanol led to a deactivation of the catalyst, but in a less extent with ethanol, as illustrated in Figure 3A. Interestingly, at 450 °C, the deactivation of NH_3 oxidation properties was again associated with the formation of oxidized compounds, mainly NO (no N_2O was recorded). NO was emitted in a lower extent at 400 °C, but similar evolutions of the ammonia conversion were observed depending on the Na loading, as illustrated in Figure S5 (Supplementary Materials).

The NO oxidation rates recorded at 450 °C depending on the sodium loading are depicted Figure 3B. Whatever the test, the NO oxidation rate remained low, with a maximum of 30% recorded with sodium free $Cu_{6.1}$/FER. Indeed, as expected, the highest NO oxidation activities were observed for

the highest loaded copper catalyst [18,19]. With the sodium free $Cu_{2.8}$/FER sample, the NO oxidation rate was limited at 7%. Addition of sodium by impregnation in water led first to an improvement of the NO oxidation rate, until 18% for 5400 ppm Na, but the rate then decreased down to 14% for approximately 2% Na. On the contrary, no influence of the Na content was observed when the alkali element was added by impregnation in ethanol. Results differed on $Cu_{6.1}$/FER catalyst: Na addition led to a similar decrease in the oxidation behavior whatever the impregnation solvent. Note that the same tendencies were observed at lower temperatures (data not shown). Finally, the sodium impregnation in water or ethanol resulted in similar trends than those observed for NH_3 oxidation. Especially, the redox function appeared not affected on the $Cu_{2.8}$/FER sample when Na was added in ethanol.

Concerning the general influence of Na addition in water, in copper-exchanged zeolite, various assumption can be advanced to explain why NH_3 and NO oxidation properties were enhanced over $Cu_{2.8}$/FER, whereas opposite results emerged over higher copper content material ($Cu_{6.1}$/FER). Indeed, the increase in NO oxidation behavior of copper-exchanged zeolite is commonly attributed to the formation of bulk copper (CuO), whether by thermal aging or copper loading increase [18,19].

In fact, when sodium was added by impregnation in water, the XRD patterns pointed out the appearance of CuO for $Cu_{2.8}$/FER while the intensity of the CuO peaks significantly increased for $Cu_{6.1}$/FER. On the contrary, no evolution of the XRD patterns was observed when sodium was added in ethanol. Consequently, the increase in oxidation properties after Na addition in water over $Cu_{2.8}$/FER could be attributed to the formation of CuO while the observed decrease in oxidation behavior for $Cu_{6.1}$/FER could be attributed to CuO sintering. A copper migration from exchange location to extra-framework, leading to CuO formation can be then suspected. After impregnation in ethanol, only copper sintering of extra-framework copper species can be postulated (after Na addition, samples were hydrothermally aged at 700 °C for 16 h).

In order to gain more information about of the sodium poisoning effects toward the copper state, especially depending on the Na solvent, samples were thereafter characterized by H_2-TPR and NO adsorption monitored by FT-IR.

2.3.2. Temperature Programmed Reduction by Hydrogen (H_2-TPR)

Generally, for copper-exchanged-based zeolites, two reductions peaks are expected. The first one is attributed to the reduction of Cu^{2+} species to Cu^{+} and the second one at higher temperature corresponds to the reduction of Cu^{+} to Cu^{0} [20]. However, for some zeolites, such as Cu/Faujasite (FAU), two H_2 consumption peaks related to the reduction of Cu^{2+} to Cu^{+} can be detected, depending of the location of the copper in the zeolite [21]. In case of extra-framework copper, the direct reduction of CuO species into metallic copper can be observed in the 200–400 °C temperature range [20,22]. In addition, coper aluminate species ($CuAl_2O_4$) may be formed if traces of extra-framework aluminum (EFAL) remains in the zeolite samples, due for instance to dealumination caused by hydrothermal treatments. $CuAl_2O_4$ reduction by H_2 should then occurs around 500 °C [23]. Besides, it was reported that the reduction temperature of exchanged copper species are depending on the zeolite Si/Al ratio, with a decrease in the reduction peak temperature with the increase of the Si/Al ratio [24]. Moreover, the temperatures of copper reduction also decrease with the increase the sodium content as cocation [20,24].

Obviously, no reduction peak was observed for the host Ferrierite zeolite (results not shown). Figure 4 reports the TPR profiles of $Cu_{2.8}$/FER and $Cu_{6.1}$/FER TPR samples depending on the Na loading for Na addition performed in water. For all catalysts, the measured H_2/Cu ratio based on hydrogen consumption until 1000 °C was always very close to 1 (Table 1). It indicates a total Cu^{2+} to Cu^{0} reduction, whatever the copper and sodium loadings. Consequently, there is neither evidence of copper stabilization in Cu^{I} state nor reduction of other species than Cu^{2+}, such as carbonates associated with Na addition for instance.

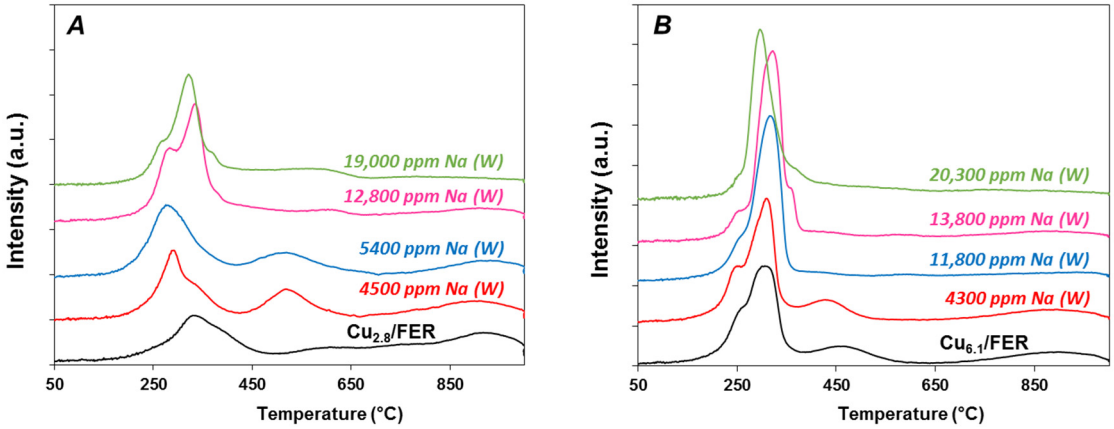

Figure 4. H_2-TPR profiles: Effect of Na loading impregnated in water (W) on (**A**) copper-exchanged zeolite $Cu_{2.8}$/FER and (**B**) on over-exchanged zeolite $Cu_{6.1}$/FER.

The $Cu_{2.8}$/FER reduction profile (Figure 4A) presents two main reduction peaks centered at 330 °C and 950 °C, and a broad reduction peak in the 500–800 °C temperature range. Varying copper loading and calcinations temperature (results not shown), the two main peaks at 330 °C and 950 °C are attributed to the two steps reduction process of exchanged Cu^{2+} via intermediate formation of Cu^{+}. The species reduced between 500 °C and 800 °C are assigned to $CuAl_2O_4$ (trace of dealumination leading to alumina was suggested by IR skeleton T-O-T characterization, Figure S2 in Supplementary Materials). However, different species of Cu^{2+} and Cu^{+} may be also reduced in this temperature range [23,25].

After addition of 4500 ppm Na by impregnation in water ($Cu_{2.8}$/FER), the first peak corresponding to the reduction of exchanged Cu^{2+} to Cu^{+} was shifted to lower temperature, at 290 °C. The reduction peak assigned to the second-step of Cu^{+} reduction to Cu^{0} is still observed at higher temperature (T = 950 °C), but the corresponding H_2 consumption was decreased compared with the sodium free sample. It became lower than for the reduction peak associated to the first reduction-step. Additionally, reduction peak centered at 520 °C was then well defined in the intermediate temperature range which corresponds to the reduction of $CuAl_2O_4$ species. Same evolutions were observed with the increase in the sodium contents, with a continuous decrease in the high temperature peak consumption (950 °C) in favor of the 250–450 °C region hydrogen consumption. The intermediate reduction peak was more or less well defined depending on the Na loading.

The $Cu_{6.1}$/FER sample exhibited TPR profiles with a first reduction-step with two components (T = 250 °C (shoulder) and 300 °C, Figure 4B). Extra-framework copper was expected for these sample since for 100% exchange (Cu/Al = 0.5), the copper loading should be around 4.5 wt. % copper. Then, the first reduction peak contained Cu^{2+} and CuO reduction. The second peak around 460 °C can be associate with copper aluminate and the last peak at 900 °C corresponds to the second step of exchanged copper reduction, from Cu^{+} to Cu^{0}. Again, addition of sodium by impregnation in water led to the disappearance of the high temperature reduction peak while the H_2 consumption in the 200–300 °C temperature range increased.

Based on this results and literature data, H_2-TPR profiles were deconvoluted to assess to the copper distribution (Figure S6): the H_2 consumption related to the peak centered at around 950 °C (attributed to Cu^{+} in exchanged position) was deduced to the integration of the broad low reduction peak(s). The remaining H_2 consumption was attributed to the one step bulk CuO reduction. In accordance with the XRD characterizations, H_2 consumptions attributed to CuO species increased with the sodium loadings. The intermediate temperature range reduction was attributed to copper aluminates reduction. However, this peak was not always well defined and some H_2 consumptions were then difficult to

address and not attributed. Finally, the copper distribution deduced from these deconvolutions are reported in Figure 5.

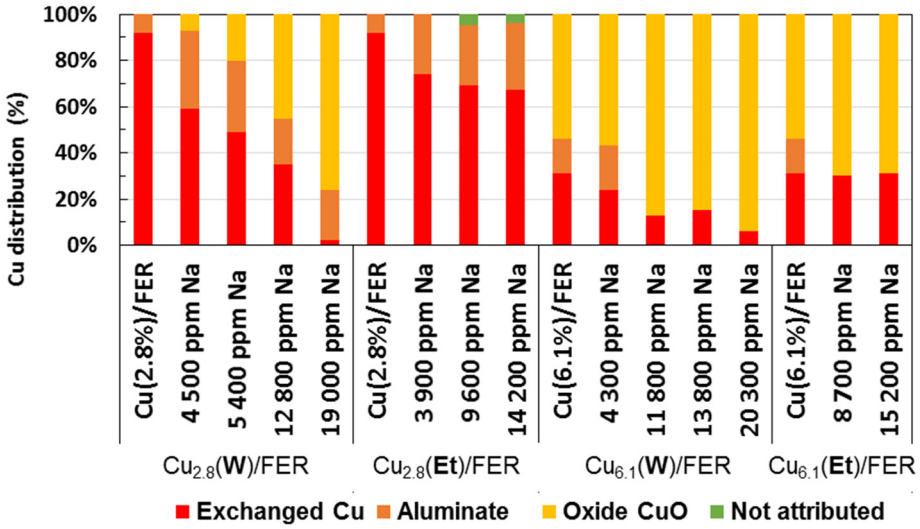

Figure 5. Copper distribution deduced from H_2-TPR experiments in function of Na impregnation solvent (water (W) or ethanol (Et)) over $Cu_{2.8}$/FER and $Cu_{6.1}$/FER catalysts. (■): exchanged Cu; (■): aluminate Cu; (■): oxide Cu; (■): no attributed.

For the sodium free $Cu_{2.8}$/FER sample, more than 90% of copper appeared to be in exchanged position. No CuO was evidenced, only few percent of copper aluminate were deduced from the deconvolution of the TPR profile. After addition of 4500 ppm Na (in water), only 60% of copper remained in exchange position, whereas approximately 33% corresponded to aluminate and 7% to CuO. Increasing the sodium loadings did not significantly affect the ratio of copper aluminate anymore, but it led to the disappearance on exchanged Cu^{2+} in favor of CuO.

Before sodium addition, the $Cu_{6.1}$/FER catalyst exhibited around 31% of exchange copper, 15% of aluminate and 54% of CuO. Again, it clearly appears that the amount of exchanged copper decreased with a remarkable continuous drop with Na loading (water as solvent), in favor of CuO formation. For instance, the amount of exchanged copper in $Cu_{6.1(W)}$/FER sample dropped to 24% with 4300 ppm Na and only 7% with 20,300 ppm of sodium.

These results are in accordance with the assumption previously postulated about the oxidation behavior of the corresponding catalysts (Section 2.3.1). After Na impregnation with water as solvent, the highest NO and NH_3 oxidation activities is correlated with the presence of copper oxide (CuO). During this impregnation procedure, sodium and copper probably compete to take place in the exchange positions. Consequently, part of the exchanged copper was moving out the zeolite framework, leading to the formation of extra-framework CuO and possibly $CuAl_2O_4$ due to the presence of traces of alumina.

When sodium amounts were added using ethanol as impregnation solvent, results significantly differ.

On $Cu_{2.8}$/FER sample (H_2-TPR profiles not shown), the Na addition in ethanol did not led to a shift the reduction temperatures of Cu^{2+} to Cu^+ and Cu^+ to Cu^0. However, a reductions peak appeared at 520 °C. It represents around 25% of hydrogen consumed for each sample containing sodium and can be attributed to $CuAl_2O_4$. Then, a quarter of the initially exchanged copper migrated out the framework and react with residual alumina. A weak peak was also observed near 740 °C (excepted for 3900 ppm of Na). The corresponding hydrogen consumption was only 2% of the total hydrogen consumption and its attribution is not clear. It is reported as "not attributed" in Figure 5. Interestingly, the hydrogen consumption of the first peak ($Cu^{2+} \rightarrow Cu^+$) was very close to the hydrogen consumption

of the highest temperature reduction peak ($Cu^{+} \rightarrow Cu^{0}$), indicating that there is no clear evidence of CuO formation, as illustrated in Figure 5.

Same trends were observed for $Cu_{6.1}$/FER catalyst. Figure 5 show that sodium impregnation in ethanol led only to small changes in copper distribution. Especially, no supplementary CuO formation was observed.

Finally, it appears that sodium impregnation in ethanol led to significantly lower interaction with exchanged copper than using water as sodium salt solvent. Using water, the amount of exchanged copper continuously decreased with the Na loading, leading to CuO formation. On the opposite, the sodium impregnation in ethanol did not significantly affect the copper distribution

In the next section, the copper state was also examined by NO adsorption monitored by FT-IR spectroscopy.

2.3.3. NO Adsorption Monitored by FT-IR Spectroscopy

Copper species in Cu-exchanged zeolite were largely studied in the literature by FT-IR adsorption experiments of probe molecules [26]. NO molecule is commonly used to investigate the oxidation state of copper cations in zeolites, due to its ability to form stable nitrosyl adducts with both Cu^{2+} and Cu^{+} cations. Several types of Cu species can co-exist, as solvated $(Cu^{2+}–(OH)^{-})^{+}$ ions [27] or Cu^{2+} monomers or $(Cu^{2+}–O^{2-}–Cu^{2+})^{2+}$ dimmers [28].

IR spectra of adsorbed NO on the Na-free catalysts containing 2.8% and 6.1% Cu are reported in Figure 6A. The interaction between NO and Cu/FER resulted in the formation of two nitrosyl complexes [Cu^{2+}–NO and Cu^{+}–NO]. The main IR bands at 1905–1910 cm^{-1} are characteristic of NO adsorbed on Cu^{2+} ions. NO adsorbed on Cu^{+} ions led to nitrosyl species at around 1810 cm^{-1} [29]. The presence of Cu^{+} sites may result from the high vacuum applied for the FT-IR experiments. However, similar copper species distribution, namely Cu^{2+} and Cu^{+} sites, were observed over both samples with 2.8% and 6.1% copper. Dinitrosyl species were not observed.

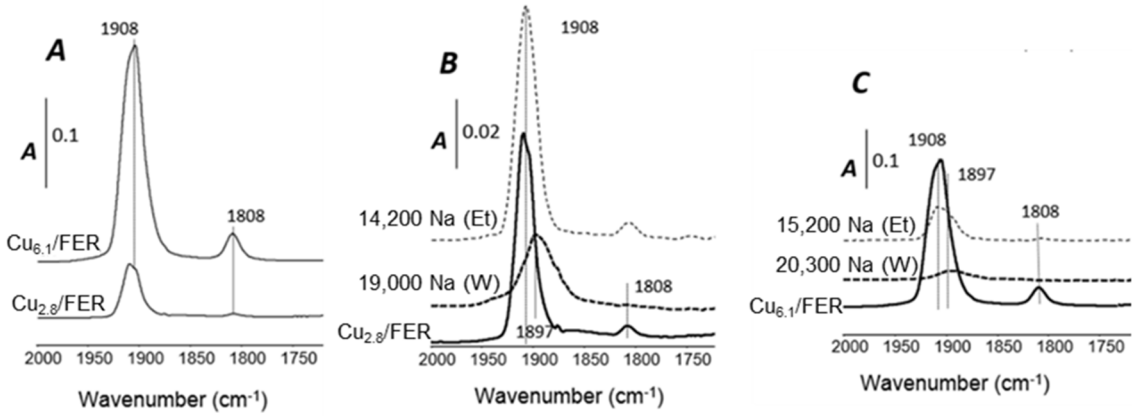

Figure 6. FT-IR spectra of NO adsorption. (**A**) comparison of Na-free copper-exchanged zeolite; (**B**) effect of Na deposit depending on the solvent over $Cu_{2.8}$/FER; (**C**) effect of Na deposit depending on the solvent over $Cu_{6.1}$/FER.

The effect of Na impregnation solvent over Cu species of $Cu_{2.8}$/FER and $Cu_{6.1}$/FER is presented in Figure 6B,C, respectively. Note that only the highest soda-content materials were examined.

For the $Cu_{2.8}$/FER catalyst (Figure 6B), similar IR bands were observed after impregnation of Na in ethanol. Notably, characteristic IR bands of NO adsorbed on Cu^{2+} ions were still observed, in similar intensity. These results are in good agreement with H_2-TPR experiments which revealed that Na impregnation in ethanol did not significantly impacted the copper distribution. Interestingly, Na addition in water led to opposite results since Cu^{2+} species were largely affected. More precisely, the band at 1908 cm^{-1} was shifted to lower wavenumbers, at 1897 cm^{-1}. The band at 1908 cm^{-1}

is assigned to the interaction between NO and isolated Cu^{2+} ions having a square pyramidal configuration [30] whereas the component at lower wavenumbers, at around 1897 cm^{-1}, is attributed to Cu^{2+} sites with a square planar configuration and adjacent to a single framework aluminum atom. It only appeared after sodium addition in water which highlights interactions between Na and exchanged copper using this solvent. The band at 1808 cm^{-1}, assigned to nitrosyl species adsorbed on Cu^{+} ion, was not observed.

Over $Cu_{6.1}$/FER samples (Figure 6C), similar tendencies were denoted: the impregnation of Na in water affected copper species more than Na addition in ethanol. Again, the band at 1897 cm^{-1} was observed denoting an alteration of copper configuration.

Finally, NO adsorption monitored by FT-IR spectroscopy confirmed that Na deposit by water pathway impacted more severely the copper species than with the ethanol route. These results globally converge with H_2-TPR experiments. However, NH_3-SCR activity also depends on NH_3 adsorption, mainly linked with acidic properties. This point is investigated in the next section.

2.4. Effect of the Na Additions on the Surface OH Groups and NH_3 Adsorption Capacity

The influence on the Na deposits on surface OH groups and ammonia adsorption ability were studied by infrared spectroscopy.

2.4.1. OH Groups

Figure 7A reports the IR spectra in OH stretching vibration region of $Cu_{2.8}$/FER and $Cu_{6.1}$/FER samples before sodium addition and for the highest sodium contents depending on the Na impregnation solvent. After activation (450 °C), IR spectra recorded at RT were characterized by IR band at 3747 cm^{-1} assigned to a single terminal Si–OH groups. The component at 3724 cm^{-1} is assigned to the O–H stretchings of geminal silanols and/or weakly perturbed vicinal pairs of terminal silanols [31]. One tailed band for bridged Al–(OH)–Si hydroxyls at 3602 cm^{-1} was also denoted. This is characteristic of the Ferrerite zeolite Brønsted acid sites, associated with the 8 and 10-membered ring channels. The band at 3642 cm^{-1} is assigned to Al–OH extra-framework groups. Thermal treatments procedures can partially remove aluminum from the crystal framework. It is assumed that the aluminum removed from the framework (EFAL) induces Lewis acidity and/or basic properties [32,33].

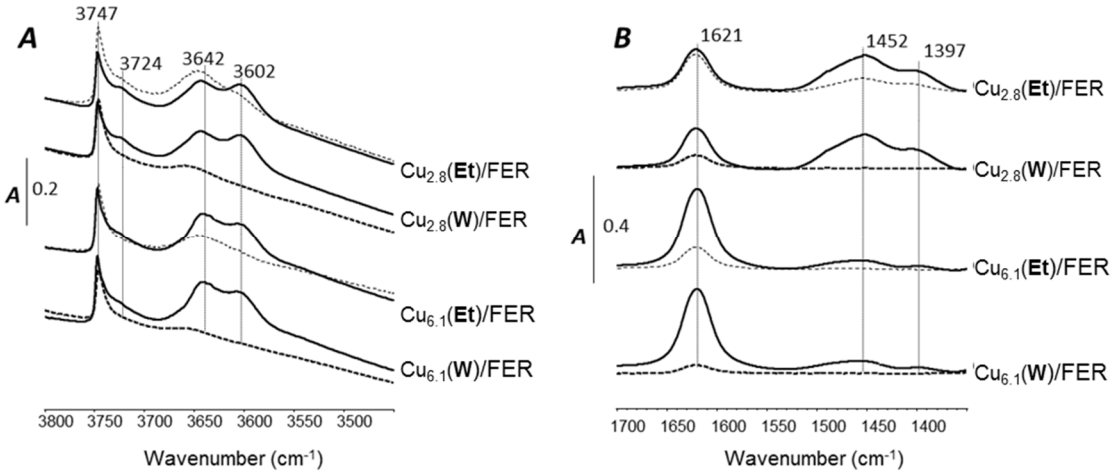

Figure 7. IR spectra for sodium free zeolites (full line) and for the highest Na contents depending on the Na solvent (water, bold dotted line; ethanol, thin dotted line). (**A**) OH stretching vibration recorded at RT after activation and evacuation at 450 °C; (**B**) IR spectra of adsorbed NH_3 after evacuation at 150 °C.

For both catalysts, impregnation of around 2% Na in water (bold dotted line) led to a significant decrease in the OH bands intensity (3602 and 3642 cm^{-1}), especially for bridged Al–(OH)–Si hydroxyls. Therefore, it could be supposed that a large part of the H^+ ions in the zeolite framework was exchanged by Na^+ ions during the impregnation. Additionally, the intensity of the band at 3602 cm^{-1} preferentially decreased with the Na loading (spectra not shown). To the opposite, Na impregnation in ethanol (thin dotted line) affected in a lesser extent the intensity of the band at 3602 cm^{-1} attributed to acidic Brønsted sites in the zeolite lattice. Consequently, it clearly appears that Na deposit in water poisoned more strongly the Brønsted acidity of the zeolite, whatever the Cu content ($Cu_{2.8}$/FER or $Cu_{6.1}$/FER samples), than for samples poisoned with ethanol as solvent for Na impregnation. Consequently Na deposited in ethanol is suspected to interact mainly with extra-framework aluminum.

Note that no supplementary bands were observed after Na impregnation, to the opposite of Fritz et al. who observed a new band at 3695 cm^{-1}, attributed to Na^+ interaction with water hydrogen-bonded to a framework oxygen atom [34].

2.4.2. NH_3 Adsorption

NH_3 adsorption was monitored by FT-IR. In the 3500–3000 cm^{-1} spectral range (spectra not shown), IR spectra were distinguished by bands at 3356, 3273, 3220 and 3189 cm^{-1} assigned to N–H stretching vibration modes [1,35–37]. More precisely, the band at 3189 cm^{-1} is assigned to Cu^+–NH_3 [38,39]. The spectral region of N–H stretching vibrations was relatively complex, because the distortion of the NH_3 molecule upon coordination led to a splitting of the $\nu_{N-H,asym}$ mode and to the activation of the $\nu_{N-H,sym}$ mode. In fact, the symmetric N–H vibration (ν_{sym}) of NH_4^+ is inactive toward IR vibration modes. Below 1800 cm^{-1} (Figure 7B), resolved N–H bending modes of ammonia adsorbed on Brønsted and Lewis sites appeared. This spectral range is dominated by absorption bands at 1452 and 1397 cm^{-1} (δ_{asym}), which are usually assigned to ammonium ions formed by the protonation of ammonia molecules located at Brønsted acid sites. These two components are tentatively assigned to different types of hydrogen-bonded ammonium, including monodentate and bidentate complexes for instance. The sharp band at 1621 cm^{-1} is assigned to bending modes of ammonia coordinatively bound to Lewis acid sites (δ_{asym}). The nature of these sites could be either tricoordinated Al atoms or Al species attached to defective sites, related to framework and extra-framework positions and also copper Lewis sites such as Cu^{2+} [1].

The bands at 1452–1397 cm^{-1} and 1621 cm^{-1} were used to determine the Brønsted and Lewis ammonia adsorption sites, based on the molar extinction coefficient values ($\varepsilon_{Brønsted}$ = 4.6 $cm \cdot \mu mol^{-1}$, ε_{Lewis} = 1.1 $cm \cdot \mu mol^{-1}$ both determined at the laboratory by successive addition of controlled amount of NH_3). The calculated amounts depending on the catalyst and the sodium loading and impregnation procedure are reported in Figure 8 (Lewis to Brønsted acid sites ratio is provided in Table 1). This graph shows a decrease in the adsorption of ammonia with increasing the Na content whatever the considered catalyst and the Na introduction mode. Considering the linear trend, one Na atom led to the disappearance of about two sites of ammonia adsorption (including Lewis and Brønsted), as previously mentioned for other materials [40]. However, Na addition led to some small different behavior in function of copper loading. For $Cu_{2.8}$/FER catalyst, the total amount of acid sites was globally not affected until 300–400 $\mu mol\ Na/g_{catalyst}$ (7000–9000 ppm Na). To the opposite, adsorbed ammonia of the catalyst containing over-exchanged copper ($Cu_{6.1}$/FER sample) is globally linearly poisoned by Na. Interestingly, the discrimination of the Brønsted and Lewis acid sites concentration also indicates that impregnation in water induced the total disappearance of the Brønsted sites for approximately 12,000 ppm Na, while the Lewis/Brønsted ratio appeared not affected when Na was added using ethanol (Table 1).

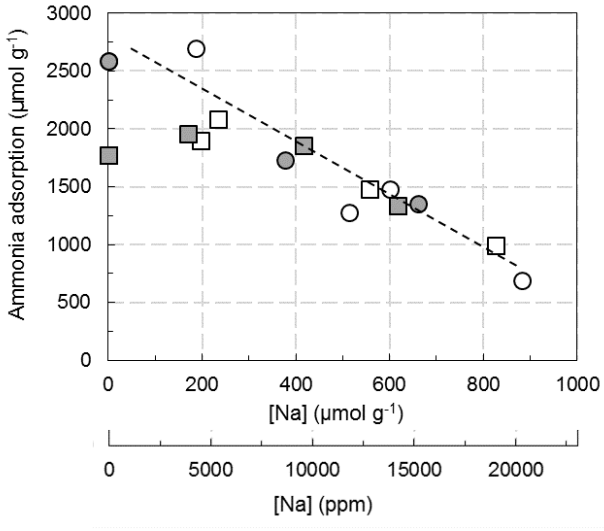

Figure 8. Relationship between the ammonia adsorption amount (determined by NH_3 adsorption evacuated at 50 °C) and the Na loading. □: $Cu_{2.8}$(W)/FER; ■: $Cu_{2.8}$(Et)/FER; ○: $Cu_{6.1}$(W)/FER; ●: $Cu_{6.1}$(Et)/FER.

Finally, FT-IR characterizations indicate a decrease in the ammonia adsorption capacity with increasing the Na content whatever the considered Na solvent. However, addition of around 2% Na in water resulted in a significant decrease in the OH bands intensity, whereas Na impregnation in ethanol affected in a lesser extent acidic Brønsted sites in the zeolite lattice. Water appeared to favor an ion exchange between the H^+ species and Na^+ ions during the impregnation step, as suspected between Na^+ and Cu^{2+} from TPR and XRD experiments.

3. Discussion

3.1. Ammonia Adsorption and Copper State

The previous sections showed that sodium additions impacted both the copper state and the acidity/ammonia adsorption behaviors.

The influence of Na addition on the ammonia adsorption capacity is rather similar depending on the impregnation procedure, and differed a little in regard on the copper loading (Figure 8).

On the opposite, significant differences were obtained concerning the copper distribution depending on the Na loading and impregnation solvent. Water solvent appeared to favor CuO formation at the expense of exchange Cu^{2+} (Figure 5).

The amount of exchanged copper determined from H_2-TPR results is reported in function of ammonia adsorption behavior in Figure 9. This figure reveals that roughly, lower the number of ammonia adsorption sites on Na poisoned sample by impregnation in water, lower the copper in exchange position for both $Cu_{2.8}$/FER (square white symbol) and $Cu_{6.1}$/FER samples (circle white symbol). No clear trend is denoted for Na impregnation in ethanol (grey symbol) because the amount of copper in exchanged position varied in a significantly lower extent. As a result, it is assumed that ammonia adsorption sites poisoned by Na deposits by ethanol route did not directly modify the nature of copper sites, whatever the materials ($Cu_{2.8}$/FER or $Cu_{6.1}$/FER). Additionally, the catalyst containing lower copper content ($Cu_{2.8}$/FER) is more sensitive to Na poisoning than $Cu_{6.1}$/FER sample which already exhibited large ratio of CuO before Na addition.

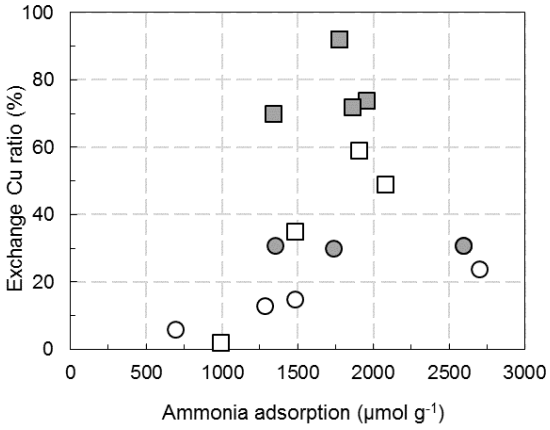

Figure 9. Relationship between the ratio of copper in exchanged position and the amount of adsorbed ammonia. □: $Cu_{2.8}$(W)/FER; ■: $Cu_{2.8}$(Et)/FER; ○: $Cu_{6.1}$(W)/FER; ●: $Cu_{6.1}$(Et)/FER.

3.2. Effect of Na Deposit over NH_3-SCR Behaviour

As presented in the introduction section, NH_3-SCR activity generally depends on both redox and acidity behaviors. Results presented in this study showed that both are potentially affected by sodium addition. In order to present a general overview of the influence of the Na addition, the $deNO_x$ activity recorded in Standard and Fast-SCR at selected temperatures (250 °C and 500 °C) for both $Cu_{2.8}$/FER and $Cu_{6.1}$/FER are plotted in function of (i) the ratio of exchanged Cu (assessed from H_2-TPR experiments) (Figure 10A,C) or (ii) the amount of adsorbed NH_3 determined by FT-IR analysis (Figure 10B,D).

At low temperature (250 °C, Figure 10A,B), the $deNO_x$ activity appeared to be sensitive to both copper state and amount of ammonia adsorption sites. More specifically, NO_x conversion increased with the ratio of copper in exchanged position until approximately 50% of exchanged copper, and became relatively constant for higher values for both Standard and Fast-SCR condition. In parallel, a linear trend was obtained between the number of ammonia adsorption sites and the $deNO_x$ efficiency in the whole studied domain, whatever the considered $Cu_{2.8}$/FER or $Cu_{6.1}$/FER samples. Additionally, as expected, Fast-SCR condition allowed higher NO_x conversion than Standard-SCR condition, but the same trends were observed for both reaction mixtures. Thus, at low temperature, it appeared that the number of ammonia adsorption sites has potentially more influence than the copper state (redox behavior). These results are consistent with the NO and NH_3 oxidation properties previously discussed in Section 2.3.1 who exhibited very low activities at 250 °C.

$DeNO_x$ activity at high temperature (500 °C) are reported in Figure 10C,D depending on the copper state and the number of ammonia adsorption sites, respectively. Obviously, obtained trends at 500 °C differ compared to those observed at low temperature. The $deNO_x$ efficiency was then strongly dependent of the ratio of exchanged copper, whatever the considered catalyst (Figure 10C). Indeed, large CuO particles (mainly on $Cu_{6.1}$/FER catalyst) favors the ammonia oxidation at high temperature, then inhibiting the NO_x reduction.

Concerning the role of the ammonia adsorption ability, trends are not clearly evidenced. Plots are largely dispersed for $Cu_{2.8}$/FER. For $Cu_{6.1}$/FER sample, a trend seems to appear with a decrease in the $deNO_x$ activity with the decrease in the number of ammonia adsorption sites, but to a limited extend. Such results could be expected since the ammonia interaction with adsorption sites (mainly acidic sites) should be very weak at this temperature. As a consequence, the activity is mostly driven by copper state at 500 °C.

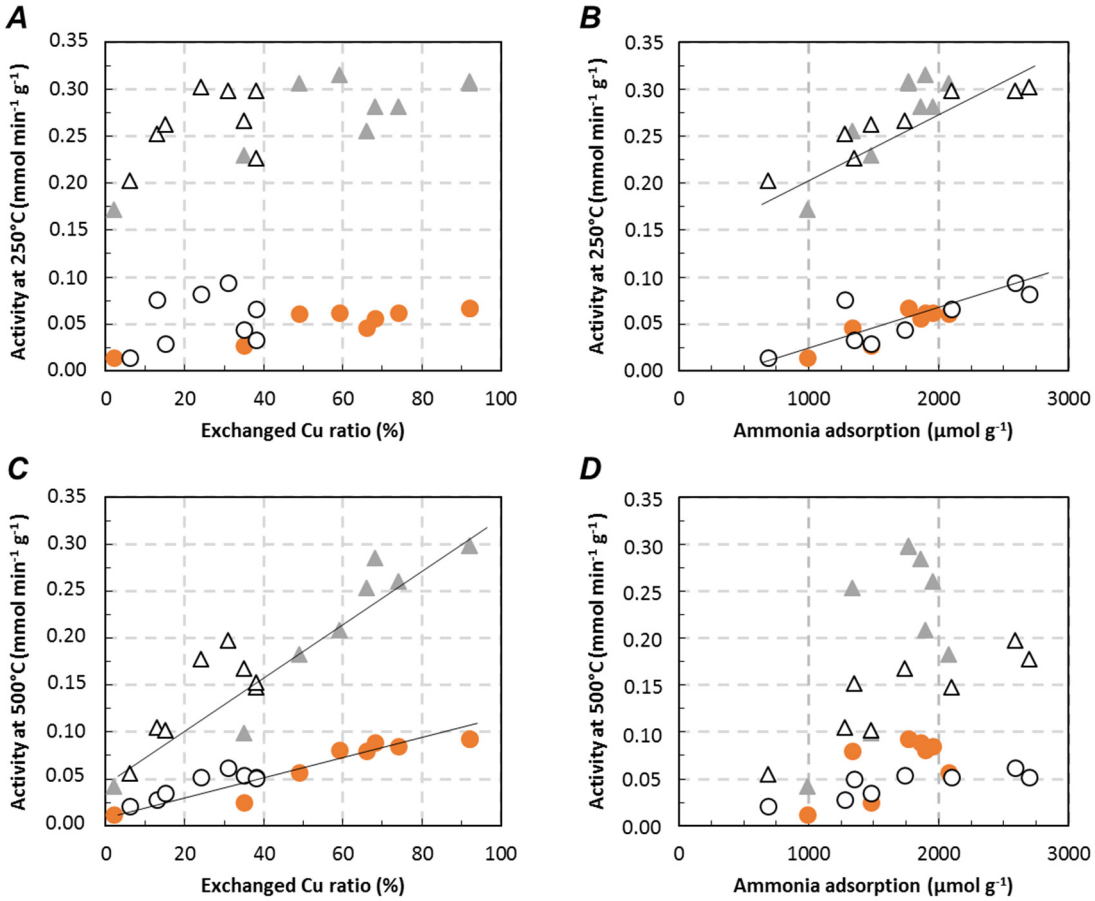

Figure 10. Effect of copper content of $Cu_{2.8}$/FER (●, ▲) and $Cu_{6.1}$/FER (○, △) catalysts in the relationship between deNOx activity in Standard-SCR (○) and Fast-SCR (△) and exchanged Cu ((**A**) 250 °C; (**C**) 500 °C) or ammonia adsorption ((**B**) 250 °C, (**D**) 500 °C).

4. Materials and Methods

4.1. Catalyst Preparation

A ferrierite structure zeolite (SiO_2/Al_2O_3 = 20, Alfa Aesar, Haverhill, MA, USA), which exhibits a channel system of 10 and 8 member rings, was selected to ensure a high hydrothermal stability. Two copper loadings were prepared (2.8 wt. % and 6.1 wt. %, measured by ICP elemental analysis after preparation of the samples) in order to obtain samples with or without extra-framework copper. Copper was added using the ion-exchange method. The ion exchanges were realized with 10 g of zeolite in suspension in $Cu(CH_3COO)_2$ (Sigma-Aldrich, L'Isle d'Abeau, France) diluted in ultra-pure water. The pH was adjusted at 5 with HNO_3 to ensure the ionic copper state, based on the diagram of copper speciation from Ajmal et al. [41]. The solution was stirred under reflux at 80 °C for 23 h. Solution was then filtered and thoroughly washed with ultra-pure water and dried at 120 °C for 15 h. The resulting powder was firstly treated at 600 °C under 10% O_2-90% N_2 for 30 min (heating rate: 2 °C min^{-1}). Vapor water (10%) was then added and the catalyst was maintained at 600 °C for 16 h before cooling to room temperature. The corresponding stabilized samples are denoted $Cu_{2.8}$/FER and $Cu_{6.1}$/FER depending on the copper content.

4.2. Sodium Addition

Sodium addition was made by impregnation, using water or ethanol as solvent. 1.5 g of the catalyst was suspended in 4 mL of water or ethanol with the desire amount of sodium ($NaNO_3$, from

Fisher Scientific Labosi, Elancourt, France). The solution was stirred at room temperature during 4 h. After solvent evaporation, the sample was dried one night at 80 °C. Finally, the resulting powder, as the catalyst without sodium, was submitted again to the thermal treatment: 30 min at 600 °C under 10% O_2-90% N_2 and 16 h at 600 °C under 10% O_2, 10% H_2O and N_2. The effective Na contents were measured by ICP, and the amount of sodium deposit was up to 20,300 ppm.

The resulting impregnated catalysts were denoted (W) or (Et) depending on the sodium impregnation solvent (water or ethanol).

4.3. Characterization Techniques and Catalytic Tests

4.3.1. Structural/Textural Characterizations, Elemental Analysis

Elemental analysis was carried out to assess the copper and sodium loadings. After mineralization of the samples, analysis were performed with an ICP-OES apparatus (Perkin Elmer Optima 2000 DV, Waltham, MA, USA).

Specific surface areas were determined by BET method (Micromeritics ASAP 2000, Norcross, GA, USA) using nitrogen adsorption at 77 K. The total pore volume was evaluated at $P/P^0 = 0.97$, and the microporous volume was calculated with t-plot. Prior to the N_2 physisorption, the samples were degassed under vacuum 1 h at 90 °C and 4 h at 350 °C.

The powder XRD patterns were collected using an Empyrean (PANalytical, Almelo, The Netherlands) diffractometer. Data acquisition was recorded from 5° to 70° (2θ) with a scanning step of 0.017. Crystalline phases were identified by comparison with ICDD database files.

4.3.2. Catalytic Activity

The SCR tests were performed in a tubular quartz reactor. For the Standard-SCR catalytic tests, 50 mg of zeolite (sieved in the 0.2–0.4 mm range) diluted in 50 mg of SiC (Prolabo, 0.35 mm) were used. The reactant gas composition was 500 ppm NO, 500 ppm NH_3, 10% O_2, 10% CO_2, 9% H_2O balanced in N_2. The total flow rate was fixed at 250 mL min^{-1}. For the Fast-SCR catalytic tests, 500 ppm NO_x were made of 250 ppm NO and 250 ppm NO_2, and only 15 mg of zeolite diluted in 15 mg of SiC were used in order to obtain conversions allowing the discrimination of catalysts. Gaseous NO, NO_2, NH_3, CO_2, O_2 and N_2 flows were adjusted by mass-flow controllers, while H_2O was added via a saturator. The composition of the feed gas and effluent stream were analyzed online with a MKS 2030 Multigas infrared analyzer.

4.3.3. Redox Properties

Temperature Programmed Reduction (TPR) with Hydrogen

Temperature programmed reduction experiments were performed on a Micromeritics Autochem 2920. Sample (100 mg) was placed in a U-shaped quartz reactor. Prior the reduction, the catalyst was in situ calcined at 450 °C for 30 min under O_2 (heating rate: 5 °C·min^{-1}). After cooling to room temperature and purge under argon flow for 45 min, the reduction was carried out under 1% H_2/Ar up to 1000 °C (rate: 10 °C·min^{-1}). The reduction was followed by a thermal conductivity detector (TCD). Because this TCD is sensitive to water, a H_2O trap was added downstream the reactor, allowing the quantification of the H_2 consumption.

NO and NH_3 Oxidation

The NO and NH_3 oxidation tests were performed in similar condition than the Standard-SCR tests. 50 mg of catalyst (sieved in the 0.2–0.4 mm range), diluted in 50 mg of SiC (Prolabo, 0.35 mm) were used. The gas compositions were 500 ppm NO or 500 ppm NH_3, 10% O_2, 10% CO_2, 9% H_2O balanced with N_2, with a total flow rate fixed at 250 mL·min^{-1}.

4.3.4. Adsorption of Probe Molecules Monitored by FT-IR

Adsorption of probe molecules monitored by infrared spectroscopy was used to characterize (i) ammonia adsorption behavior (the usual pyridine sensor to characterize acidic sites is not appropriate since it is not able to diffuse into the small porosity of the considered materials [31,42]) and (ii) copper state of exchanged zeolites by NO adsorption. IR spectra were collected using a Nexus Nicolet spectrometer equipped with a DTGS detector (deuterium triglyceride sulfur) and a KBr beam splitter. Spectra were normalized to a disc of 10 $mg \cdot cm^{-2}$. Before adsorption, the catalyst was in situ pre-treated under vacuum at 450 °C. Ammonia was then adsorbed at 25 °C and desorption was performed up to 450 °C. NO adsorption was performed at room temperature, IR spectra are compared with the same n_{NO}/n_{Cu} (≈30%) by adding a known amount of NO on the cell.

5. Conclusions

The impact of sodium, as alkali poison from biodiesel, was investigated on two model NH_3-SCR catalysts ($Cu_{2.8\%}$/FER and $Cu_{6.1\%}$/FER), depending on the Na introduction method (impregnation in water or in ethanol). Impregnation in ethanol led mainly to a decrease in ammonia adsorption capacity, which affected the deNO_x efficiency at low temperature whereas NO and NH_3 oxidation behaviors were not really affected. Impregnation of Na in water (representative of interaction of catalyst with condensed water, which occurs during engine stop and cold start) furthermore caused a migration of copper species from the exchange sites to extra-framework CuO. Consequently, NH_3 and NO oxidation behaviors were decreased. Finally, whatever the catalyst and the reaction mixture (Fast or Standard-SCR), the NO_x conversion decrease with Na addition appeared linked to the decrease in ammonia adsorption at low temperature (250 °C), whereas the activity at high temperature (500 °C) mainly depended on the ratio of exchanged copper.

Supplementary Materials: The following are available online at www.mdpi.com/2073-4344/8/1/3/s1, Figure S1: XRD patterns of fresh and hydrotreated zeolite for 16 h at 600 °C and 750 °C. Figure S2: T–O–T bands obtained with zeolite before and after hydrotreatment at 600 °C and 750 °C during 16 h (samples diluted in KBr). Figure S3: XRD patterns of fresh FER, sodium free $Cu_{2.8}$/FER and $Cu_{2.8}$(w)/FER with 19,000 ppm Na impregnated in water. Figure S4: XRD patterns of fresh FER, sodium free $Cu_{6.1}$/FER and $Cu_{6.1}$(w)/FER with 20,300 ppm Na impregnated in water. Figure S5: Effect of Na loading on NH_3 oxidation at 400 °C over $Cu_{2.8}$/FER and $Cu_{6.1}$/FER samples depending on the Na loading impregnated in water (W) or ethanol (Et). Figure S6: H_2-TPR profile deconvolution over $Cu_{2.8}$/FER with 19,000 ppm of Na content impregnated in water.

Acknowledgments: The authors gratefully acknowledge the French National Agency for Research (ANR) for its financial support (Appibio Project, Reference ANR-14-CE22-0003).

Author Contributions: Xavier Courtois, Fabien Can, Vincent Lauga and Eduard Emil Iojoiu conceived and designed the experiments, Marie-Laure Tarot and Mathias Barreau performed the experiments; Marie-Laure Tarot analyzed the data, Marie-Laure Tarot, Xavier Courtois and Fabien Can wrote the paper, Daniel Duprez, Vincent Lauga and Eduard Emil Iojoiu also contributed to scientific discussions.

Conflicts of Interest: The authors declare no conflict of interest.

References

1. Wang, D.; Zhang, L.; Li, J.; Kamasamudram, K.; Epling, W.S. NH_3-SCR over Cu/SAPO-34—Zeolite acidity and Cu structure changes as a function of Cu loading. *Catal. Today* **2014**, *231*, 64–74. [CrossRef]
2. Ma, L.; Cheng, Y.; Cavataio, G.; McCabe, R.W.; Fu, L.; Li, J. Characterization of commercial Cu-SSZ-13 and Cu-SAPO-34 catalysts with hydrothermal treatment for NH_3-SCR of NO_x in diesel exhaust. *Chem. Eng. J.* **2013**, *225*, 323–330. [CrossRef]
3. Kwak, J.H.; Tonkyn, R.G.; Kim, D.H.; Szanyi, J.; Peden, C.H.F. Excellent activity and selectivity of Cu-SSZ-13 in the selective catalytic reduction of NO_x with NH_3. *J. Catal.* **2010**, *275*, 187–190. [CrossRef]
4. Kim, Y.J.; Lee, J.K.; Min, K.M.; Hong, S.B.; Nam, I.-S.; Cho, B.K. Hydrothermal stability of CuSSZ13 for reducing NO_x by NH_3. *J. Catal.* **2014**, *311*, 447–457. [CrossRef]
5. Brandenberger, S.; Kröcher, O.; Tissler, A.; Althoff, R. The state of the art in selective catalytic reduction of NO_x by ammonia using metal-exchanged zeolite catalysts. *Catal. Rev.* **2008**, *50*, 492–531. [CrossRef]

6. Guan, B.; Zhan, R.; Lin, H.; Huang, Z. Review of state of the art technologies of selective catalytic reduction of NO_x from diesel engine exhaust. *Appl. Therm. Eng.* **2014**, *66*, 395–414. [CrossRef]
7. Nicosia, D.; Czekaj, I.; Kröcher, O. Chemical deactivation of $V_2O_5/WO_3–TiO_2$ SCR catalysts by additives and impurities from fuels, lubrication oils and urea solution: Part II. Characterization study of the effect of alkali and alkaline earth metals. *Appl. Catal. B* **2008**, *77*, 228–236. [CrossRef]
8. Klimczak, M.; Kern, P.; Heinzelmann, T.; Lucas, M.; Claus, P. High-throughput study of the effects of inorganic additives and poisons on NH_3-SCR catalysts—Part I: $V_2O_5–WO_3/TiO_2$ catalysts. *Appl. Catal. B* **2010**, *95*, 39–47. [CrossRef]
9. Chen, L.; Li, J.; Ge, M. The poisoning effect of alkali metals doping over nano $V_2O_5–WO_3/TiO_2$ catalysts on selective catalytic reduction of NO_x by NH_3. *Chem. Eng. J.* **2011**, *170*, 531–537. [CrossRef]
10. Kern, P.; Klimczak, M.; Heinzelmann, T.; Lucas, M.; Claus, P. High-throughput study of the effects of inorganic additives and poisons on NH_3-SCR catalysts. Part II: Fe–zeolite catalysts. *Appl. Catal. B* **2010**, *95*, 48–56. [CrossRef]
11. Shwan, S.; Jansson, J.; Olsson, L.; Skoglundh, M. Chemical deactivation of H-BEA and Fe-BEA as NH_3-SCR catalysts—Effect of potassium. *Appl. Catal. B* **2015**, *166–167*, 277–286. [CrossRef]
12. Ma, J.; Si, Z.; Weng, D.; Wu, X.; Ma, Y. Potassium poisoning on Cu-SAPO-34 catalyst for selective catalytic reduction of NO_x with ammonia. *Chem. Eng. J.* **2015**, *267*, 191–200. [CrossRef]
13. Brookshear, D.W.; Nguyen, K.; Toops, T.J.; Bunting, B.G.; Rohr, W.F. Impact of Biodiesel-Based Na on the Selective Catalytic Reduction of NO_x by NH_3 over Cu–Zeolite Catalysts. *Top. Catal.* **2013**, *56*, 62–67. [CrossRef]
14. Brookshear, D.W.; Nguyen, K.; Toops, T.J.; Bunting, B.G.; Rohr, W.F.; Howe, J. Investigation of the effects of biodiesel-based Na on emissions control components. *Catal. Today* **2012**, *184*, 205–218. [CrossRef]
15. Rahkamaa-Tolonen, K.; Maunula, T.; Lomma, M.; Huuhtanen, M.; Keiski, R.L. The effect of NO_2 on the activity of fresh and aged zeolite catalysts in the NH_3-SCR reaction. *Catal. Today* **2005**, *100*, 217–222. [CrossRef]
16. Hamon, C.; Blanchard, G. Device for Treating Exhaust Gases. European Patent EP 2857084 A1, 8 April 2015.
17. Lezcano-Gonzalez, I.; Deka, U.; van der Bij, H.E.; Paalanen, P.; Arstad, B.; Weckhuysen, B.M.; Beale, A.M. Chemical deactivation of Cu-SSZ-13 ammonia selective catalytic reduction (NH_3-SCR) systems. *Appl. Catal. B* **2014**, *154–155*, 339–349. [CrossRef]
18. Sultana, A.; Nanba, T.; Haneda, M.; Sasaki, M.; Hamada, H. Influence of co-cations on the formation of Cu^+ species in Cu/ZSM-5 and its effect on selective catalytic reduction of NO_x with NH_3. *Appl. Catal. B* **2010**, *101*, 61–67. [CrossRef]
19. Mihai, O.; Widyastuti, C.R.; Andonova, S.; Kamasamudram, K.; Li, J.; Joshi, S.Y.; Currier, N.W.; Yezerets, A.; Olsson, L. The effect of Cu-loading on different reactions involved in NH_3-SCR over Cu-BEA catalysts. *J. Catal.* **2014**, *311*, 170–181. [CrossRef]
20. Bulánek, R.; Wichterlová, B.; Sobalík, Z.; Tichý, J. Reducibility and oxidation activity of Cu ions in zeolites: Effect of Cu ion coordination and zeolite framework composition. *Appl. Catal. B* **2001**, *31*, 13–25. [CrossRef]
21. Delahay, G.; Valade, D.; Guzmán-Vargas, A.; Coq, B. Selective catalytic reduction of nitric oxide with ammonia on Fe-ZSM-5 catalysts prepared by different methods. *Appl. Catal. B* **2005**, *55*, 149–155. [CrossRef]
22. Delahay, G.; Coq, B.; Broussous, L. Selective catalytic reduction of nitrogen monoxide by decane on copper-exchanged beta zeolites. *Appl. Catal. B* **1997**, *12*, 49–59. [CrossRef]
23. Dumas, J.M.; Geron, C.; Kribii, A.; Barbier, J. Preparation of supported copper catalysts. *Appl. Catal. B* **1989**, *47*, L9–L15. [CrossRef]
24. Torre-Abreu, C.; Ribeiro, M.F.; Henriques, C.; Delahay, G. NO TPD and H_2-TPR studies for characterisation of CuMOR catalysts the role of Si/Al ratio, copper content and cocation. *Appl. Catal. B* **1997**, *14*, 261–272. [CrossRef]
25. Severino, F.; Brito, J.L.; Laine, J.; Fierro, J.L.G.; Agudo, A.L. Nature of copper active sites in the carbon monoxide oxidation on $Cual_2O_4$ and $cucr_2o_4$ spinel type catalysts. *J. Catal.* **1998**, *177*, 82–95. [CrossRef]
26. Deka, U.; Lezcano-Gonzalez, I.; Weckhuysen, B.M.; Beale, A.M. Local environment and nature of Cu active sites in zeolite-based catalysts for the selective catalytic reduction of NO_x. *ACS Catal.* **2013**, *3*, 413–427. [CrossRef]
27. Dědeček, J.; Wichterlová, B. Role of hydrated Cu ion complexes and aluminum distribution in the framework on the Cu ion siting in ZSM-5. *J. Phys. Chem. B* **1997**, *101*, 10233–10240. [CrossRef]

28. Costa, P.D.; Modén, B.; Meitzner, G.D.; Lee, D.K.; Iglesia, E. Spectroscopic and chemical characterization of active and inactive Cu species in NO decomposition catalysts based on Cu-ZSM5. *Phys. Chem. Chem. Phys.* **2002**, *4*, 4590–4601. [CrossRef]
29. Henriques, C.; Ribeiro, M.F.; Abreu, C.; Murphy, D.M.; Poignant, F.; Saussey, J.; Lavalley, J.C. An FT-IR study of NO adsorption over Cu-exchanged MFI catalysts: Effect of Si/Al ratio, copper loading and catalyst pre-treatment. *Appl. Catal. B* **1998**, *16*, 79–95. [CrossRef]
30. Hadjiivanov, K.I. Identification of neutral and charged N_x O_y surface species by IR spectroscopy. *Catal. Rev.* **2000**, *42*, 71–144. [CrossRef]
31. Trombetta, M.; Busca, G.; Rossini, S.; Piccoli, V.; Cornaro, U.; Guercio, A.; Catani, R.; Willey, R.J. FT-IR studies on light olefin skeletal isomerization catalysis: III surface acidity and activity of amorphous and crystalline catalysts belonging to the SiO_2–Al_2O_3 system. *J. Catal.* **1998**, *179*, 581–596. [CrossRef]
32. Chakarova, K.; Hadjiivanov, K. FTIR study of N_2 and CO adsorption on H-D-FER. *Microporous Mesoporous Mater.* **2013**, *177*, 59–65. [CrossRef]
33. De Ménorval, B.; Ayrault, P.; Gnep, N.S.; Guisnet, M. Mechanism of n-butene skeletal isomerization over HFER zeolites: A new proposal. *J. Catal.* **2005**, *230*, 38–51. [CrossRef]
34. Fritz, P.O.; Lunsford, J.H. The effect of sodium poisoning on dealuminated Y-type zeolites. *J. Catal.* **1989**, *118*, 85–98. [CrossRef]
35. Datka, J.; Gil, B.; Kubacka, A. Acid properties of NaH-mordenites: Infrared spectroscopic studies of ammonia sorption. *Zeolites* **1995**, *15*, 501–506. [CrossRef]
36. Kosslick, H.; Berndt, H.; Lanh, H.D.; Martin, A.; Miessner, H.; Tuan, V.A.; Jänchen, J. Acid properties of ZSM-20-type zeolite. *J. Chem. Soc. Faraday Trans.* **1994**, *90*, 2837. [CrossRef]
37. Elzey, S.; Mubayi, A.; Larsen, S.C.; Grassian, V.H. FTIR study of the selective catalytic reduction of NO_2 with ammonia on nanocrystalline NaY and CuY. *J. Mol. Catal. A* **2008**, *285*, 48–57. [CrossRef]
38. Poignant, F.; Saussey, J.; Lavalley, J.-C.; Mabilon, G. In situ FT-IR study of NH_3 formation during the reduction of NO_x with propane on H/Cu-ZSM-5 in excess oxygen. *Catal. Today* **1996**, *29*, 93–97. [CrossRef]
39. Poignant, F.; Saussey, J.; Lavalley, J.-C.; Mabilon, G. NH_3 formation during the reduction of nitrogen monoxide by propane on H–Cu–ZSM-5 in excess oxygen. *J. Chem. Soc. Chem. Commun.* **1995**, *89–90*. [CrossRef]
40. Can, F.; Travert, A.; Ruaux, V.; Gilson, J.-P.; Maugé, F.; Hu, R.; Wormsbecher, R.F. FCC gasoline sulfur reduction additives: Mechanism and active sites. *J. Catal.* **2007**, *249*, 79–92. [CrossRef]
41. Ajmal, M.; Hussain Khan, A.; Ahmad, S.; Ahmad, A. Role of sawdust in the removal of copper(II) from industrial wastes. *Water Res.* **1998**, *32*, 3085–3091. [CrossRef]
42. Wichterlová, B.; Tvarůžková, Z.; Sobalík, Z.; Sarv, P. Determination and properties of acid sites in H-ferrierite: A comparison of ferrierite and MFI structures. *Microporous Mesoporous Mater.* **1998**, *24*, 223–233. [CrossRef]